Laser and Particle Beams (2002), *20*, 195–199. Printed in the USA.

DOI: 10.1017/S0263034602202062

Application of novel techniques for interferogram analysis to laser–plasma femtosecond probing

P. TOMASSINI,[1] A. GIULIETTI,[1] L.A. GIZZI,[1] R. NUMICO,[1] M. GALIMBERTI,[2] D. GIULIETTI,[2] AND M. BORGHESI[3]

[1]Intense Laser Irradiation Laboratory–IPCF CNR, Area della Ricerca di Pisa, Via G. Moruzzi, 1 56124 Pisa, Italy
[2]Intense Laser Irradiation Laboratory–IPCF CNR, Dipartimento di Fisica Universitá di Pisa and I.N.F.M unitá di Pisa, Pisa, Italy
[3]Department of Pure and Applied Physics, The Queen's University, Belfast, UK

(RECEIVED 15 November 2001; ACCEPTED 18 December 2001)

Abstract

Recently, two novel techniques for the extraction of the phase-shift map (Tomassini *et al.* (2001). *Applied Optics* **40**, 35) and the electronic density map estimation (Tomassini P. & Giulietti A. (2001). *Optics Communication* **199**, 143–148) have been proposed. In this article, we apply both methods to a sample laser–plasma interferogram obtained with femtoseconds probe pulse, in an experimental setup devoted to laser particle acceleration studies.

Keywords: Abelinversion; Continuous wavelet transforms; Interferometry; Particle acceleration; Plasma diagnostics

1. INTRODUCTION

The phase-shift extraction from interferogram images is generally performed via a straightforward method based on fast Fourier transforms (FFT; Takeda *et al.*, 1982). This method is fast and generally very effective, but it can fail in producing accurate phase-shift maps in facing low quality fringe structures. Unfortunately, the number of physical processes that can degrade the fringe visibility is very large. Even if the effects of some of these sources can be strongly reduced with refinement of the interferometry techniques (e.g., in the case of uncorrelated noise in the image, nonuniform illumination, etc.) or a reduction of the probe duration (in the case of fringe smearing due to the plasma evolution), the effect of the deviation of the probe light due to strong electronic density gradients cannot be eliminated in the interferometer acquisition step. As a result, the standard FFT technique hardly works properly when applied to interferograms of very steep density gradients. Recently (Tomassini *et al.*, 2001), a new method to extract the phase-shift map from interferograms has been proposed. The new method, interferogram analysis via continuous wavelet transform ridge extraction (IACRE), takes advantage of the combined spatial and spectral resolution of the continuous wavelet transforms (CWT; Holschneider, 1995) to identify the fringe structures, and results are more flexible, accurate, and robust than standard FFT-based ones.

Once the phase-shift map has been obtained, one has to use the Abel Inversion to retrieve the 2D electronic density map. The Abel Inversion method is based on the strong assumption that the full 3D electronic density is axisymmetric along an axis parallel to the interferometry plane. This assumption is often poorly verified and if we force in using Abel Inversion, we can introduce large errors in the density map, especially near the best estimated symmetry axis. In a recent procedure (Tomassini & Giulietti, 2001), Abel Inversion has been generalized and can be applied to density distributions with a moderate asymmetry. As a corollary, this generalized Abel Inversion provides a first step in 3D density map extraction.

In this article, we show the preliminary results of the analysis of interferograms obtained with femtosecond laser pulses probing plasmas produced by the exploding foils technique. The set of interferograms has been produced in order to characterize the plasma before, during, and after the passage of a ultrastrong laser pulse, in an experimental setup devoted to the study of the production of multi-megaelectron volt electrons generated by laser–plasma interactions (Giulietti *et al.*, 2001).

Address correspondence and reprint requests to: Paolo Tomassini, Intense Laser Irradiation Laboratory–IPCF CNR, Area della Ricerca di Pisa, Via G. Moruzzi, 1 56124 Pisa, Italy. E-mail: tomassini@ifam.pi.cnr.it

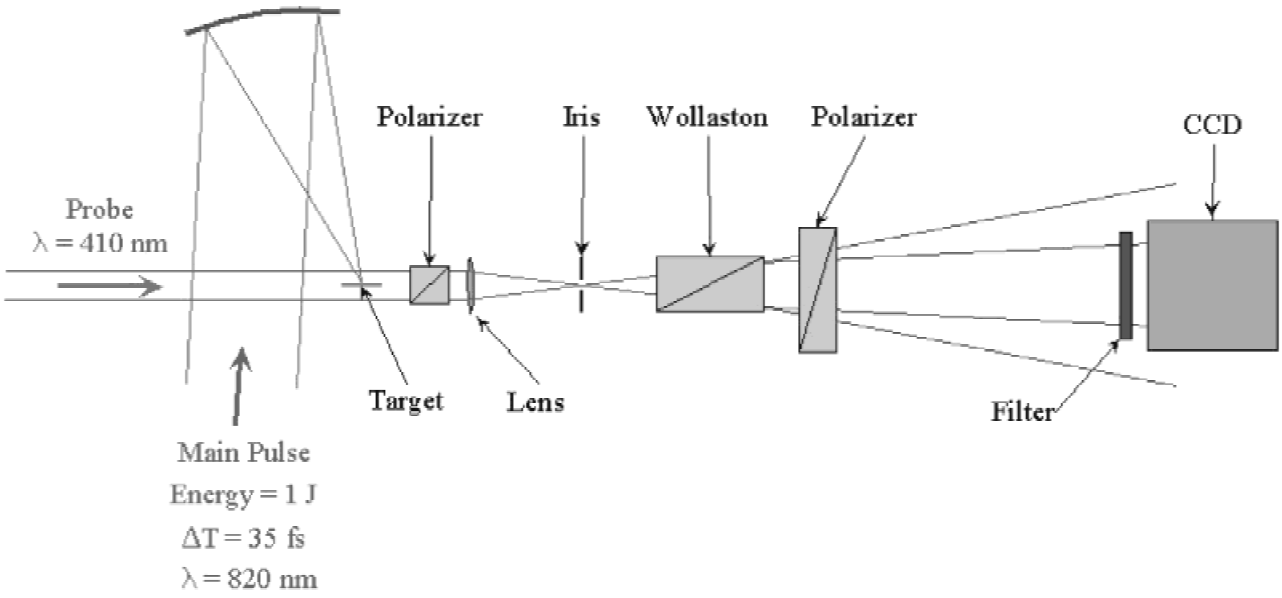

Fig. 1. Interferometer setup: A modified Nomarski interferometer has been used to generate digital interferometry images. A probe pulse (a fraction of the second harmonic of the main pulse) probes the plasma perpendicularly to the symmetry axis.

2. INTERFEROMETRY SETUP

The experiment has been performed on the Salle Jaune of the Laboratoire d'Optique Appliquee with a laser pulse of wavelength 0.82 μm delivering 1 J in 35 fs. A portion of the pulse has been doubled in frequency with a KDP crystal (probe pulse) and the remaining portion (main pulse) has been focused with an off-axis parabola on the target, a thin foil of FORMVAR (see Fig. 1).

The nanosecond amplified spontaneous emission (ASE) which precedes the main pulse makes the foil explode in the focal spot. As a consequence, the main pulse interacts with a preformed plasma of peak density well below the critical density and of scalelength of a few tens of microns.

The interferometry pulse probes the plasma in a direction parallel to the plastic foil, that is, perpendicular to the plasma expansion axis, which is also roughly the plasma symmetry axis. A modified Nomarski interferometry setup (Benattar *et al.*, 1979) is used to generate the interferometry images on a CCD camera (see Figs. 1 and 2).

3. THE PHASE-SHIFT EXTRACTION WITH THE IACRE METHOD

A detailed description of the IACRE method and an accurate comparison between IACRE and the standard FFT-based methods performances has been published elsewhere (Tomassini *et al.*, 2000, 2001). In this section, we will just sketch the main steps of the novel method.

Consider the interferogram of Figure 3. It has been produced 10 ps after the interaction of a preformed plasma with a 35-fs main pulse focused on it with an intensity of 10^{20} W/cm^2.

The laser beam came from the right-hand side and the plasma is approximately symmetric along the horizontal *x*

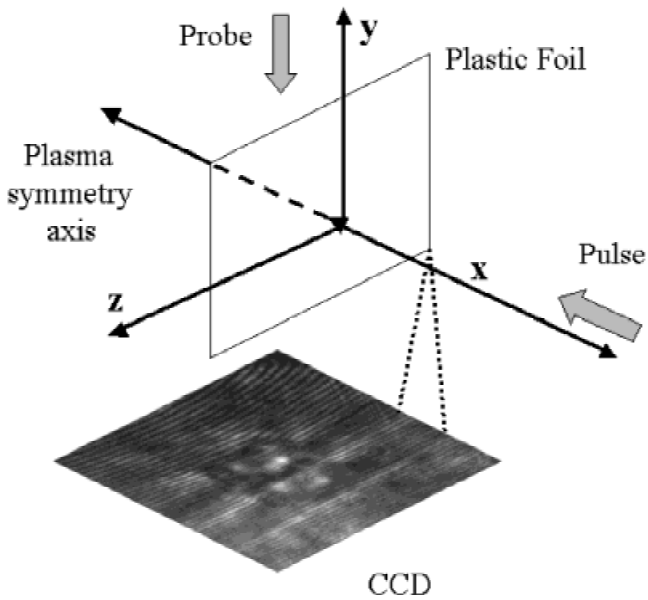

Fig. 2. A plastic foil explodes under the intense ASE radiation coming along the *x* axis. The plasma is approximately symmetrical along the *x* axis. The probe beam probes the plasma along the *y* direction and generates an interferometry image on a CCD camera.

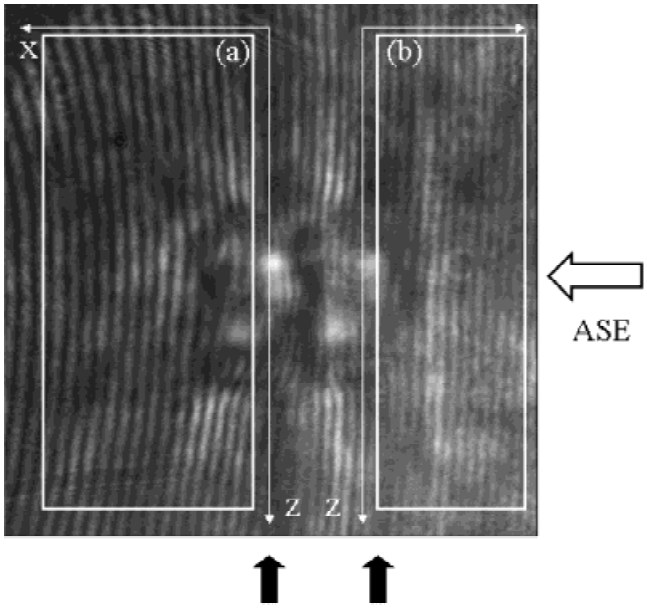

Fig. 3. Interferometry pattern of a plasma obtained from 1-μm-thick foil. The probe pulse followed the main pulse by 10 ps. The laser pulse came from the right. Boxes (a) and (b) refer to the two analyzed regions of the plasma (left and right sides of the foil target, respectively). The two images of the thin foil are indicated by the black arrows.

coordinate. Since a Nomarski interferometer produces two partially overlapped images of the region of interest, two images of the target (labeled by the two black arrows) are visible. The boxes show the two analyzed regions, one on the side of the incoming laser beam (the right one) and one on the rear side.

To apply the IACRE method to the each subimage (left and right boxes), we extract the phase shift $\delta\phi(z,x)$ as follow. For each z build a sequence $s_z(x)$ by taking the line-out of the subimage. Next,

- compute the CWT coefficients $C_s(a,b)$ of $s_z(x)$, a and b being the "voice" and "time" parameters, respectively;
- detect the "Ridge" $\mathcal{R}(C_s)$ of the C_s map, recording the phase $\phi(x)$ of the signal rebuilt with $\mathcal{R}(C_s)$;
- estimate the wavevector k_p of the unperturbed fringes and, finally, compute the phase-shift $\delta\phi(z,x)$ as

$$\delta\phi(z,x) = \phi(z,x) - k_p x. \tag{1}$$

The analysis of the test interferogram is complicated by the presence of fringe curvature also in absence of the plasma. This problem has been solved by acquiring a "Mask" interferogram (without plasma) before each shot. A phase-shift of the Mask $\delta\phi^{Mask}$ is estimated and the corrected phase-shift due to the electronic plasma density $\delta\phi^{Plasma}$ is obtained simply as

$$\delta\phi^{Plasma} = \delta\phi - \delta\phi^{Mask}. \tag{2}$$

The results for the left and right box subimages are reported in Figure 4.

The two phase-shift maps of the front (right box) and rear (left box) sides of the plasma have quite similar structures, with strong evidence of a hole in the electronic density near the target, where steep density gradients occur. These gradients are responsible for the reduction of fringe visibility at the edges of the hole.

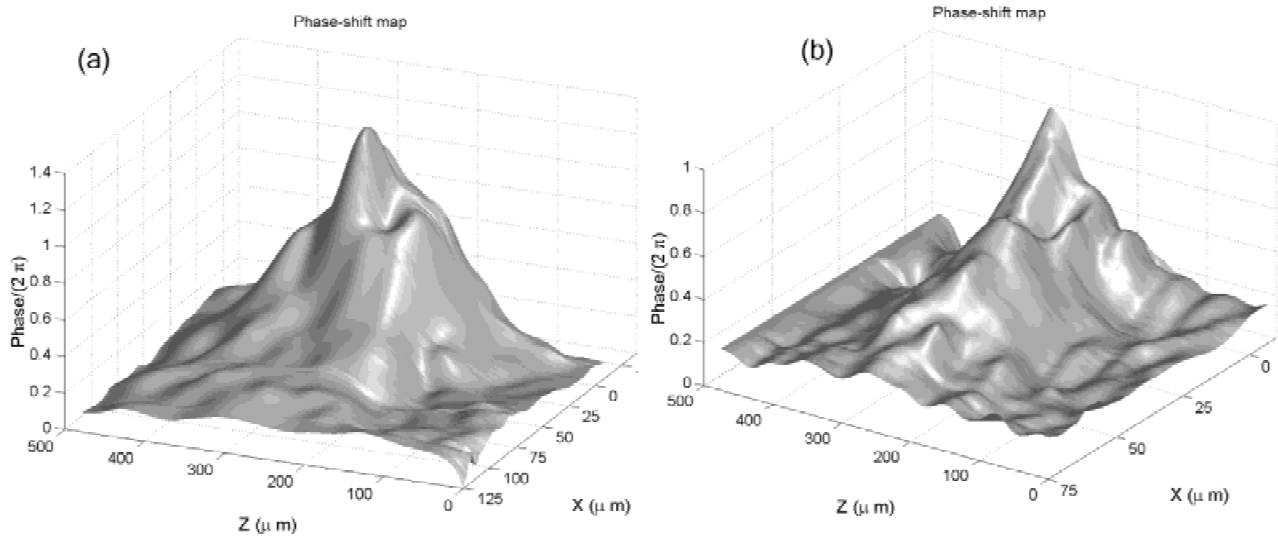

Fig. 4. Corrected phase-shift of the left (a) and right (b) boxes of Figure 3.

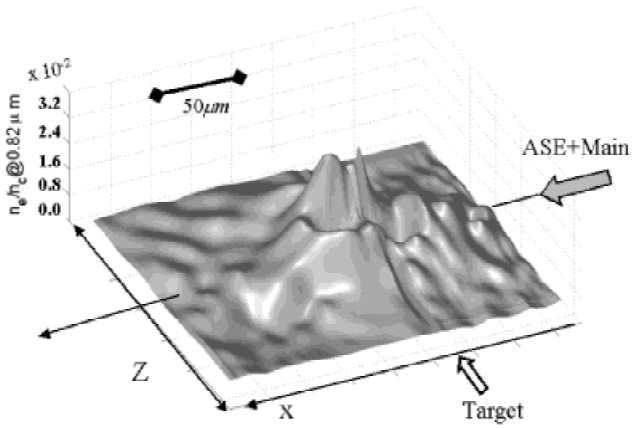

Fig. 5. Projection of the density map in the left and right boxes of the interferogram of Figure 3 onto the x–z plane. A hole in the electronic density map is apparent.

4. NONAXISYMMETRIC ABEL INVERSION

We now proceed in the estimation of the electronic density map n_e. As is clear in Figure 4, the phase-shift maps are not really mirror symmetric, so we expect that the computation of n_e via standard Abel Inversion could introduce relevant errors. We then apply the Generalized Abel Inversion (Tomassini & Giulietti, 2001) to the corrected phase-shift maps (left and right boxes) in order to minimize inversion errors. As in the standard Abel Inversion, the position z_0 of the best symmetry axis must be determined by maximizing, for example, the cross-correlation between the two half maps

$$\delta\phi^+(\zeta, x) = \delta\phi^{Plasma}(z - z_0, x) \quad z > z_0,$$
$$\delta\phi^-(\zeta, x) = \delta\phi^{Plasma}(z_0 - z, x) \quad z < z_0; \tag{3}$$

next two 2D maps $n_0(r, x)$ and $n_1(r, x)$ are numerically computed with the integrals

$$n_0(r, x) = -n_c \frac{\lambda_p}{\pi^2} \int_r^\infty d\zeta \, \frac{1}{\sqrt{\zeta^2 - r^2}} \frac{\partial}{\partial\zeta} \delta\phi_s(\zeta, x)$$
$$n_1(r, x) = -n_c \frac{\lambda_p}{\pi^2} \, r \int_r^\infty d\zeta \, \frac{1}{\sqrt{\zeta^2 - r^2}} \frac{\partial}{\partial\zeta} \left(\frac{\delta\phi_a(\zeta, x)}{\zeta} \right), \tag{4}$$

where n_c is the critical density for the probe wavelength λ_p and $\delta\phi_s$, $\delta\phi_a$ are the symmetrized and antisymmetrized half maps:

$$\delta\phi_s \equiv \frac{1}{2} (\delta\phi^+(\zeta) + \delta\phi^-(\zeta)), \qquad \delta\phi_a \equiv \frac{1}{2} (\delta\phi^+(\zeta) - \delta\phi^-(\zeta)).$$

The 3D electron density map can now be built up as follow. First, the map is mirror-symmetric along the x–z plane. This assumption is necessary because in the process of formation of the interferogram, an integration along the y direction is made. Consider then one half space (let us say

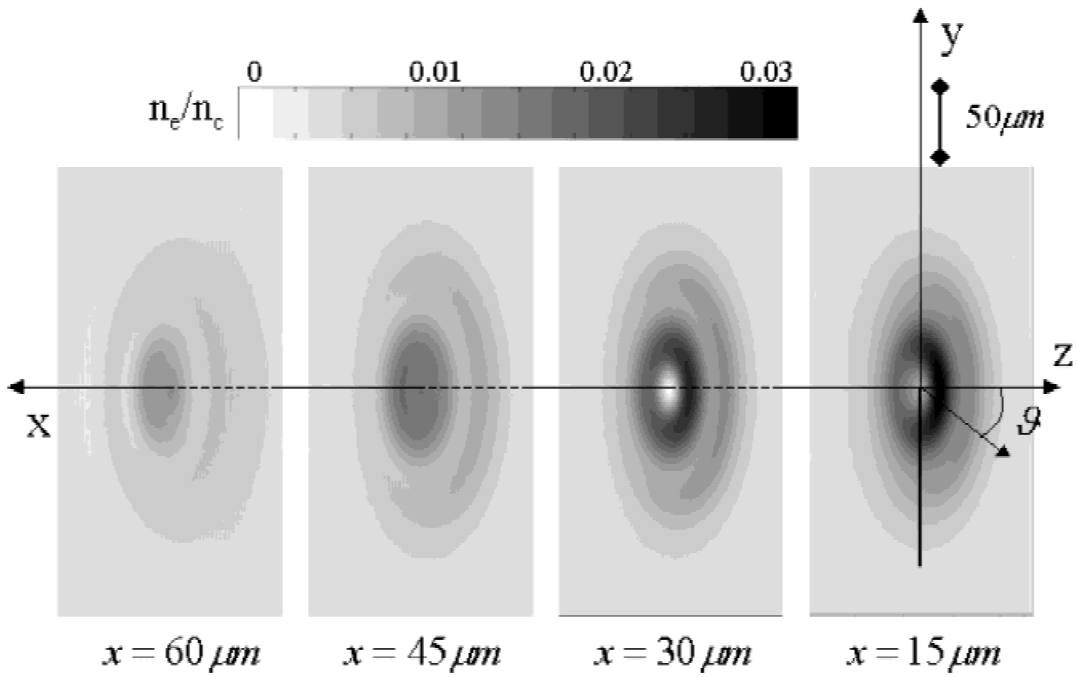

Fig. 6. Slides of the 3D electron density map in the left box of the interferogram of Figure 3. A hole in the electronic density is evident at distance from the target between $x = 15$ μm and $x = 30$ μm.

the one with y positive) and, for each x, identity a point in the y–z plane by using polar coordinates (r, θ). Finally, the 3D map

$$n(r, \theta, x) = n_0(r, x) + n_1(r, x)\cos(\theta) \quad (5)$$

represents the best estimation of the electronic density map obtained with the Generalized Abel Inversion. In Figure 5, the projection in the x–z plane of the density map at both sides of the target is reproduced, while in Figure 6, a sequence of slices of the 3D density map in the left box at constant x is shown.

The projection of the density maps onto the x–z plane (see Figs. 5 and 6) confirms the presence of a dramatic density depression (hole) along the laser propagation path, near the original target position. In Figure 6, a multiring structure in the 3D density map is evident. The presence of such a structure is confirmed by the phase-shift map of the rear side box (a). For each line-out of the map at $x = const$ in the region near the target, the phase shows a minimum for $z = 310$ μm (the position of the best symmetry axis), two almost symmetrical maxima at $z = 280$ μm and $z = 340$ μm (the inner ring in Fig. 6) and another two symmetrical maxima at $z = 250$ μm and $z = 370$ μm (the outer ring in Fig. 6).

5. COMMENTS

We applied the IACRE and Generalized Abel Inversion to a sample interferogram, obtained just few picoseconds after the interaction of an ultraintense femtosecond laser pulse with a preformed plasma from an exploding thin foil. The density map evidences the creation of a sharp electron density depression near the original target position.

We mention that the method has been also applied to a series of interferograms taken before, during, and after the propagation of the ultrarelativistic 35-fs pulse with the plasma.

The analysis is still in progress and preliminary results confirm (Tomassini *et al.*, 2001) that the IACRE method is much more robust and sensitive than standard FFT-based method, which frequently failed in producing reasonably accurate phase-shift maps. We then expect that IACRE and Generalized Abel Inversion methods will give a strong contribution in the comprehension of such an extreme laser–plasma interaction regime.

REFERENCES

Benattar, R., Popovics, M. & Siegel, R. (1979). Polarized light interferometer for laser fusion studies. *Rev. Sci. Instrum.* **50**, 1583.

Giulietti, D., Galimberti, M., Giulietti, A., Numico, R., Tomassini, P., Borghesi, M., Malka, V., Fritzler, S., Pittman, M., Ta Phouc, K. & Pukhov, A. (2002). Production of ultracollimated bunches of multi-MeV electrons by 35 fs laser pulses propagating in exploding-foil plasmas. *Phys. Plasmas* **9**(9), 3655–3658.

Holschneider, M. (1995). *Wavelet: An analysis tool*. Oxford: Clarendon Press.

Takeda, M., Ina, H. & Kobayashi, S. (1982). Fourier-transform method of fringe-pattern analysis for computer-based topography and interferometry. *J. Opt. Soc. Am.* **72**, 156.

Tomassini, P., Borghesi, M., Galimberti, M., Giulietti, A., Giulietti, D., Willi, O. & Gizzi, L.A. (2001). Analyzing laser-plasma interferograms with a Continuous Wavelet Transform Ridge Extraction technique. *Appl. Optics* **40**, 35.

Tomassini, P. & Giulietti, A. (2001). A generalization of Abel Inversion to non axisymmetric density distribution. *Opt. Comm.* **199**, 143–148.

Tomassini, P., Giulietti, A. & Gizzi, L.A. (2000). *Analyzing laser-plasma interferograms with the continuous Wavelet Transform*, IFAM-Note 2/2000, 15-11-2000, available at xray.ifam.pi.cnr.it.